Nuclear Instruments and Methods in Physics Research A 1069 (2024) 169844

Contents lists available at ScienceDirect

Nuclear Inst. and Methods in Physics Research, A

journal homepage: www.elsevier.com/locate/nima

Timepix4 characterization with monochromatic X-rays at the Elettra synchrotron facility

A. Feruglio [a], N.V. Biesuz [b], R. Bolzonella [b,c,*], L. Brombal [d,e], F. Brun [d,f], P. Cardarelli [b], V. Cavallini [b,c]

[a] Department of Physics, University of Pisa and INFN Pisa Division, Largo Bruno Pontecorvo 3, 56127, Pisa, Italy
[b] INFN, Division of Ferrara, via G. Saragat 1, 44122, Ferrara, Italy
[c] Department of Physics and Earth Science, University of Ferrara, via G. Saragat 1, 44122, Ferrara, Italy
[d] INFN, Division of Trieste, via A. Valerio 2, 34127, Trieste, Italy
[e] Department of Physics, University of Trieste, via A. Valerio 2, 34127, Trieste, Italy
[f] Department of Engineering and Architecture, University of Trieste, via A. Valerio 10, 34127, Trieste, Italy

ARTICLE INFO

Keywords:
Photon-counting detector
Hybrid pixel detector
Timepix4
Radiation imaging

ABSTRACT

Timepix4 is the latest generation application-specific integrated circuit (ASIC) of the Medipix family, developed by the Medipix4 Collaboration. A characterization of a Timepix4 assembly bump-bonded to a planar 300 μm thick silicon pixelated sensor has been performed by using monochromatic X-rays at the Elettra synchrotron facility (Trieste, Italy). In particular, a calibration of the ToT against the energy released in the Si detector has been performed for each pixel, to optimize energy resolution. A preliminary analysis to estimate the detector photon counting linearity and pixel readout dead time was also carried out.

1. Introduction

Timepix4 is the latest generation application-specific integrated circuit (ASIC) of the Medipix family, developed by the Medipix4 Collaboration, and mainly targeted for single particle detection in hybrid pixel detectors [1,2]. Several generations of chips have been developed by the Medipix collaborations since 1998, divided into ASICs part of the Medipix and Timepix families [3]. These chips have been widely used in several technologies based on imaging and particle tracking, applied in fields including high energy physics experiments, nuclear physics, medical and biology applications, and material science applications [4,5]. A characterization of a Timepix4 assembly bump-bonded to a 300 μm pixelated silicon sensor has been performed by using monochromatic X-rays at the SYRMEP beamline of the Elettra synchrotron facility [6].

2. Timepix4 ASIC and DAQ system

Timepix4 ASIC is built using 65 nm CMOS technology, and it attains high spatial and temporal resolutions, thanks to a pixel pitch of 55 μm and a Time-to-Digital Converter bin size of 195 ps. An energy resolution of about 1 keV is provided by the Time-over-Threshold (ToT) measurement. With around 230 thousand channels (448 × 512), equipped with both analog and digital front-end electronics, the Timepix4 ASIC stands out for its data-driven architecture, capable of withstanding data rates up to a bandwidth of 160 Gb/s. A SPIDR4 SoC-based external electronics [7], which also serve as a flexible control board for configuring the ASIC, ensures the management of this high data rate. A custom DAQ software has been used.

3. Energy calibration

3.1. Measurements procedure

A pixel-by-pixel energy calibration is required to convert the ToT signal into the deposited energy [8,9]. A series of flat field images have been acquired by illuminating the Si sensor bonded to the Timepix4 with monochromatic X-rays at 18 energy levels between 8.5 and 40 keV. The Si sensor has been biased at 100 V. The detector was scanned through the laminar beam at a velocity of 2 mm/s to obtain a uniform irradiation. High statistic images were collected at each energy level to limit statistical fluctuations, resulting in about 4000 hits/pixel over the full detector matrix.

3.2. Energy against ToT calibration

3.2.1. X-rays based calibration analysis

The analysis, performed with a custom software developed by INFN, consisted of filling a ToT histogram for each energy and pixel

* Corresponding author at: Department of Physics and Earth Science, University of Ferrara, via G. Saragat 1, 44122, Ferrara, Italy.
E-mail address: rbolzonella@fe.infn.it (R. Bolzonella).

https://doi.org/10.1016/j.nima.2024.169844
Received 28 June 2024; Received in revised form 7 August 2024; Accepted 4 September 2024
Available online 5 September 2024

Table 1
Results of the energy calibration. For each nominal energy, the corresponding peak ToT and $FWHM_{ToT}$/ToT, as well as the peak energy and $FWHM_E$/E after the calibration procedure are reported.

Nominal energy (keV)	8.5	11	20	40
Peak ToT (ns)	352	480	911	1832
$FWHM_{ToT}$/ToT	0.44	0.38	0.32	0.29
Peak E (keV)	8.5	11.1	20.2	40.1
$FWHM_E$/E	0.17	0.15	0.10	0.06

and fitting its peak, corresponding to the full energy of the impinging photons, with a Gaussian function. Only single pixel events have been considered; more pixels clusters have been used only to validate the calibration results, because their ToT sum would be the outcome of different pixel responses, resulting on a non-correct calibration. Moreover, single pixel have been used to allow a comparison with testpulse based calibration, as will be shown in Section 3.2.3. The resulting mean ToT values and corresponding uncertainties were fitted as a function of the nominal X-ray energy (E) with the following calibration function [9]:

$$\mathrm{ToT} = \mathrm{a} \cdot \mathrm{E} + \mathrm{b} - \frac{\mathrm{c}}{\mathrm{E} - \mathrm{t}} \tag{1}$$

where a, b, c, and t are the fit parameters. The hyperbolic term in (1) is needed to account for deviation from linearity at low energies.

3.2.2. Testpulse based calibration

In addition to the analysis with monochromatic X-rays, a calibration using the detector's internally generated test pulses has been performed in the range 4.7 to 50.7 keV. Test pulses inject a user-selectable amount of charge which is readily converted to a nominal deposited energy by considering that 3.6 eV is needed to produce one free electron in silicon. This procedure is useful since, in general, a source of tunable monoenergetic X-rays is not available in standard radiation laboratories.

3.2.3. Calibrations comparison

Compared to the X-ray-based results, the test-pulse calibration shows discrepancies which can be attributed to the uncertainty on the test pulse input capacitance on each pixel. To compensate for this difference a simple linear correction is applied to match the two calibration on the linear regions (the low energy region changes accordingly):

$$\mathrm{ToT_{TP}} = \mathrm{a_{lin}} \cdot \mathrm{E_{TP}} \cdot \mathrm{g} + \mathrm{b_{lin}} + \mathrm{h} \tag{2}$$

where $\mathrm{ToT_{TP}}$ and $\mathrm{E_{TP}}$ are the measured ToT and nominal energy for the test pulse calibration, $\mathrm{a_{lin}}$ and $\mathrm{b_{lin}}$ are the parameters of the X-ray calibration based on a fit on the linear region of the ToT vs E plot, and g and h are the correction factors. Interestingly, the pixel-by-pixel distribution of the correction factor g, shown in Fig. 1, resembles the power supply distribution across the matrix, showing this particular shape due to the wire-bonding connection used to provide power to the Timepix4. The correlation between the calibration and the power supply is still under study. Conversely, h and the other calibration parameters do not show any spatial correlation and are uniformly distributed on the pixel matrix.

3.2.4. Merged calibration improvements

After the correction, test-pulse and X-ray data can be merged, therefore extending the calibration range.

The results of the calibration at four energy levels are reported in Table 1. Further details on the energy calibration can be found in [10].

The energies resulting from the corrected calibration are compatible with the monochromatic energies. At low energies the energy is expected to have a non-linear dependency on the ToT, due to threshold effects. As expected, energy resolution improves, compared to ToT resolution, due to the correction of different pixels response.

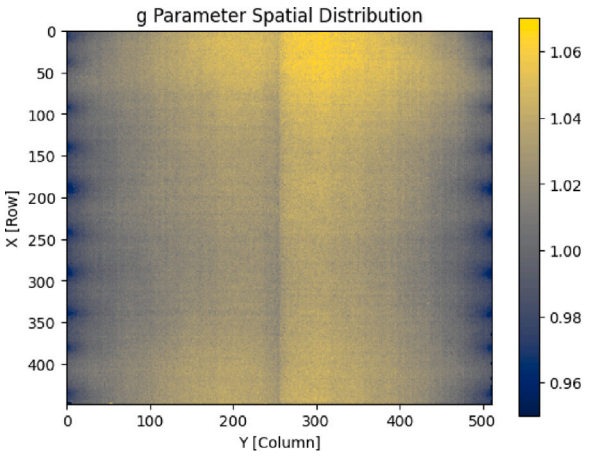

Fig. 1. Distribution across the matrix of the parameter g, used to correct the slope of the test pulse calibration based on the X-rays-based calibration. The distribution follows the power supply distribution, with this particular shape due to the wire-bond connections. The detector pixel size is 55 μm, and the overall chip sizes are 24.7 mm × 29.96 mm.

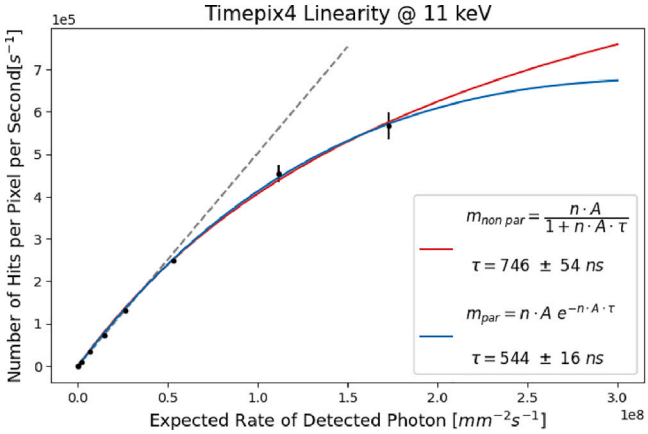

Fig. 2. Linearity plot at 11 keV evaluated over one of the three 5 × 5 pixel regions. From the plot, the linearity range and the dead time were estimated.

4. Photon counting linearity and dead time

4.1. Counting response estimation

The detector photon counting linearity was assessed by exposing the detector to increasing event rates, which were monitored through an ionization chamber. To avoid saturating the readout fast links, only three 5 × 5 pixel regions were activated during the measurement. Linearity was measured at two energy levels, namely 11 keV, at absorbed photon flux in the range $2.74 \times 10^4 \div 1.73 \times 10^8 \cdot 10^7$ hits $\cdot mm^{-2}\ s^{-1}$, and 20 keV, at absorbed photon flux in the range $1.88 \times 10^6 \div 3.24 \times 10^7 \cdot 10^7$ hits $\cdot mm^{-2} s^{-1}$. Since the pixel behavior depends directly on the number of measured hits, a clusterization of the events was not performed in this section. From the plots in Fig. 2, the linearity range is estimated to be up to $4 \cdot 10^7$ hits $\cdot mm^{-2}\ s^{-1}$ at 11 keV (up to $3 \cdot 10^7$ hits $\cdot mm^{-2}\ s^{-1}$ at 20 keV).

4.2. Readout dead time estimation

As high flux was available, linearity plots were also used to estimate the pixels readout dead time by fitting both paralyzable and non-paralyzable dead-time models [11]. At 11 keV: $\tau_{non\ par} = 745 \pm 54$ ns, $\tau_{par} = 544 \pm 15$ ns; at 20 keV: $\tau_{non\ par} = 817 \pm 67$ ns, $\tau_{par} = 760 \pm 56$ ns.

In the explored flux range, both the paralyzable and non-paralyzable models fit the data correctly. A dependence of the pixels' dead time on the energy of the acquired photons and, consequently, on the ToT of the input signals was observed.

5. Conclusions

This work proved that a ToT calibration based only on X-rays measurements or only on testpulse can be improved by merging the two methods to obtain better energy resolution performance.

Regarding the pixel readout dead time, further investigations will be performed to study this dependence and to characterize dead time as a function of different acquisition parameters, such as the Krummenacher feedback current or the pixels front-end gain mode.

Declaration of competing interest

The authors declare that they have no known competing financial interests or personal relationships that could have appeared to influence the work reported in this paper.

Acknowledgments

This work was carried out in the context of the Medipix4 Collaboration and supported by the MEDIPIX4 project funded by INFN-CSN5.

References

[1] X. Llopart, et al., Timepix4, a large area pixel detector readout chip which can be tiled on 4 sides providing sub-200 ps timestamp binning, J. Instrum. 17 (01) (2022) C01044, http://dx.doi.org/10.1088/1748-0221/17/01/C01044.

[2] V. Sriskaran, et al., High-rate, high-resolution single photon X-ray imaging: Medipix4, a large 4-side buttable pixel readout chip with high granularity and spectroscopic capabilities, J. Instrum. 19 (02) (2024) P02024, http://dx.doi.org/10.1088/1748-0221/19/02/P02024.

[3] R. Ballabriga, M. Campbell, X. Llopart, Asic developments for radiation imaging applications: The medipix and timepix family, Nucl. Instrum. Methods A 878 (2018) 10–23, http://dx.doi.org/10.1016/j.nima.2017.07.029.

[4] M. Bisogni, P. Delogu, M. Fantacci, G. Mettivier, M. Montesi, M. Novelli, M. Quattrocchi, V. Rosso, P. Russo, A. Stefanini, A Medipix2-based imaging system for digital mammography with silicon pixel detectors, IEEE Trans. Nucl. Sci. 51 (2004) 3081–3085, http://dx.doi.org/10.1109/tns.2004.839079.

[5] S. Procz, C. Avila, J. Fey, G. Roque, M. Schuetz, E. Hamann, X-ray and gamma imaging with Medipix and Timepix detectors in medical research, Radiat. Meas. 127 (2019) 106104, http://dx.doi.org/10.1016/j.radmeas.2019.04.007, URL https://www.sciencedirect.com/science/article/pii/S1350448719300599.

[6] G. Tromba, et al., The SYRMEP beamline of elettra: Clinical mammography and bio-medical applications, AIP Conf. Proc. 1266 (1) (2010) 18–23, http://dx.doi.org/10.1063/1.3478190.

[7] SPIDR4 Project, Nikhef.nl, 2024, URL https://spidr4.nikhef.nl/.

[8] D. Turecek, J. Jakubek, M. Kroupa, P. Soukup, Energy calibration of pixel detector working in time-over-threshold mode using test pulses, in: IEEE Nuclear Science Symposium Conference Record, 2011, http://dx.doi.org/10.1109/NSSMIC.2011.6154668.

[9] J. Jakubek, J. Dammer, T. Holy, M. Jakubek, S. Pospisil, V. Tichy, J. Uher, D. Vavrik, Spectrometric properties of TimePix pixel detector for x-ray color and phase sensitive radiography, in: IEEE Nuclear Science Symposium Conference Record, Vol. 3, 2007, http://dx.doi.org/10.1109/NSSMIC.2007.4436610.

[10] P. Delogu, N. Biesuz, R. Bolzonella, L. Brombal, V. Cavallini, F. Brun, P. Cardarelli, A. Feruglio, M. Fiorini, R. Longo, V. Rosso, Validation of Timepix4 energy calibration procedures with synchrotron X-ray beams, Nuclear Instruments and Methods in Physics Research Section A: Accelerators, Spectrometers, Detectors and Associated Equipment 1068 (2024) 169716, http://dx.doi.org/10.1016/j.nima.2024.169716, https://www.sciencedirect.com/science/article/pii/S0168900224006429.

[11] S. Usman, A. Patil, Radiation detector deadtime and pile up: A review of the status of science, Nuclear Eng. Technol. 50 (2018) 1006–1016, http://dx.doi.org/10.1016/j.net.2018.06.014.